IJE TRANSACTIONS A: Basics Vol. 37 No. 01, (January 2024) 56-66

International Journal of Engineering

Journal Homepage: www.ije.ir

# Experimental Study of Thermal Ageing and Hydrogen Embrittlement Effect on the Equipments of a Rocket Engine

A. Rezala*, A. Jabbar Hassan

*Mechanical and Process Engineering Faculty, University of Science and Technology Houari Boumediene (USTHB), B.P. 32, El-Alia, 16111, Bab-Ezzouar, Algiers, Algeria*

*PAPER INFO*

*Paper history:*
Received 17 January 2023
Received in revised form 22 August 2023
Accepted 23 August 2023

*Keywords*:
*Disc Pressure Tests*
*Thermal Embrittlement*
*Hydrogen Embrittlement*
*Rocket Engine*
*Fatigue Cycle*

*ABSTRACT*

In the present study employed disc pressure tests to assess the effects of hydrogen embrittlement and thermal ageing on the fatigue life of a thin-wall circular part within a rocket engine. The technique compared the pressure resistance of membranes tested under helium and hydrogen, offering a simple, sensitive, and reliable method. Disc tests were selected to mimic natural operating conditions, as they align with those of a thin-wall circular part within a rocket engine. The originality of these tests appears to lie in their enhanced performance in terms of sensitivity and reproducibility. To achieve this, tests were conducted across various conditions, including sample thicknesses of 0.75 mm, a broad range of strain rates from $10^{-6}$ $s^{-1}$ to $10^{0}$ $s^{-1}$, temperatures spanning from 20°C to 900°C, and pressure rates from $10^{-2}$ to $2.10^{4}$ MPa/min. Furthermore, a variety of materials were investigated, including copper, nickel alloy, and stainless steel. The results demonstrated that thermal aging leads to precipitation, particularly intergranular precipitation. These precipitates diminish the material's ductility, particularly when they are nearly continuous. Additionally, the material's sensitivity to hydrogen becomes significant when hydrogen, supersaturated due to rapid cooling, becomes trapped on precipitates formed at high temperatures. Furthermore, the results indicated that thermal and hydrogen-induced damage mutually reinforces each other, resulting in reduced fatigue life under high deformation.

***doi**: 10.5829/ije.2024.37.01a.06*

## 1. INTRODUCTION

Hydrogen embrittlement (HE) is a common and significant issue for various metallic materials. The challenges posed by hydrogen embrittlement are diverse, stemming from its introduction during material development, part manufacturing, and service stages. This occurs when the equipment comes into contact with hydrogen-containing gases or is exposed to hydrogen generated through corrosion, electrochemical processes, and water dissociation. The actual service environment constitutes an external factor influencing HE behavior, while the internal factor involves the accumulation of hydrogen atoms due to interactions with shallow hydrogen traps. Potential sites for these traps in martensitic materials include grain boundaries (1) and dislocations (2). Several studies have highlighted the pivotal role of hydrogen-dislocation interaction in local hydrogen accumulation and plasticity (3, 4). This phenomenon can be accelerated through the hydrogen-enhanced localized plasticity (HELP) mechanism, suggesting that trapped hydrogen in dislocations facilitates dislocation emission and movement (5).

For many metal alloys, mechanical strength, ductility, and fatigue life can be substantially reduced when exposed to hydrogen. Hydrogen-related brittle fracture becomes more intricate due to the interaction between hydrogen and stress under various loads. Wang et al.'s findings (6) demonstrated that the fracture strength of SSRT (slow strain rate tensile) at a rate of $1 \times 10^{-7}$ $s^{-1}$ surpassed the threshold strength for CLT (constant loading tensile). Introducing nanoparticles into the matrix significantly enhanced the strength of DSHS (Dual-Phase Steel) without compromising its toughness and plasticity, as these nanoparticles served as effective irreversible hydrogen traps, mitigating HE risk (7).

*Corresponding Author Email: aicha.rezala@usthb.edu.dz
(A. Rezala)

Please cite this article as: Rezala A, Jabbar Hassan A. Experimental Study of Thermal Ageing and Hydrogen Embrittlement Effect on the Equipments of a Rocket Engine. International Journal of Engineering, Transactions A: Basics, 2024;37(01): 56-66.

Qianqian et al. (8) studied the influence of adding Mo to Ti which was investigated concerning hydrogen-induced cracking behavior. They concluded that Mo addition affected the interaction between hydrogen, defects, and cracking behavior, offering insights into enhancing the hydrogen-cracking resistance of titanium alloys in structural materials. Additionally, Momotani et al. (9) revealed hydrogen accumulation at the prior austenite grain boundaries, particularly at lower strain rates ($8.3 \times 10^{-6}$ $s^{-1}$). However, the impact of temperature on hydrogen accumulation and hydrogen-induced fracture remains unclear. Literature indicates increased hydrogen diffusion rates with rising temperatures (10), while hydrogen susceptibility initially increases and then decreases (11, 12).

Extensive research into metals' sensitivity to hydrogen has led to established solutions for specific contexts. However, evolving contexts and demands for enhanced material performance necessitate further exploration without compromising hydrogen resistance. Theoretical and bibliographical approaches aid in pre-selecting materials based on numerous embrittlement parameters, though accurate qualification through tests reflecting service conditions remains essential. To mimic these conditions, Shenguang et al. (13) systematically studied hydrogen embrittlement in 15Cr martensitic stainless steel used for steam turbine blades. Slow strain rate tensile (SSRT) and constant loading tensile (CLT) tests were conducted at room temperature and 80°C.

Notably, despite lower hydrogen concentration during SSRT, the hydrogen-induced fracture strength of 15Cr steel in SSRT was lower than the threshold for CLT due to enhanced local hydrogen concentration from mobile dislocation transport during SSRT. Moreover, even with higher hydrogen concentration absorbed during SSRT at 80°C, the hydrogen embrittlement susceptibility was lower due to reduced local hydrogen accumulation at higher temperatures.

Standard techniques for characterizing metals under hydrogen conditions fall short in simulating combustion chamber behavior subjected to on-off cycles. Rocket engines, for example, experience detrimental cycles where hydrogen content increases during high-temperature usage, remains trapped during rapid cooling upon shutdown, and leads to super-saturation-induced damage during low-temperature restart. This super-saturation can shorten material fatigue life.

Additionally, thermal ageing following medium to high-temperature usage leads to uneven growth of initial precipitates, especially near grain boundaries, resulting in metallurgical embrittlement. Such embrittlement amplifies when materials are employed in hydrogen-rich atmospheres. To effectively understand hydrogen embrittlement and thermal aging effects on rocket engine fatigue life, practical service conditions must be simulated in the lab. Monotonic biaxial tests, such as gas disc pressure tests on membranes loaded by internal gas pressure, offer advantages over traditional tensile tests by providing wider temperature and strain rate ranges. The interplay of load conditions and service temperature, alongside varying materials' susceptibility to HE, is pivotal during rocket engine service.

This article introduces a specific technique for characterizing metals under hydrogen conditions using disc testing. The aim is to uncover the impacts of thermal aging and hydrogen on rocket engine service life during on-off cycles while considering multiple parameters. Moreover, numerical results are presented to enhance awareness of hydrogen-related issues among designers and analysts. This technique surpasses conventional approaches to hydrogen embrittlement, especially for equipment under severe stress like rocket engines. Materials for such engines must demonstrate low hydrogen embrittlement across broad temperature ranges. Current research primarily focuses on studying hydrogen embrittlement degradation mechanisms and thermal aging to address long-term performance demands of rocket engines.

## 2. MATERIALS AND METHODS

**2. 1. Material** Three materials have been used in the present study:

**2. 1. 1. Low-alloy Copper (CuCrZr)** DLR provided a copper alloy (Cu-0.65%Cr-0.05%Zr), which is a material with structural hardening properties. It as-delivered state, the alloy underwent a solution treatment, followed by over-aging and precipitation tempering at 450°C. The alloy, after undergoing this treatment, offers a favorable balance between high thermal conductivity and improved mechanical characteristics.

**2. 1. 2. Nickel Alloy (Inconel 600)** Imphy provided Inconel 600, a nickel-based superalloy containing (14 to 17%) chromium and (6 to 10%) iron. The melting range of this alloy falls between 1350-1410°C. This alloy exhibits good high-temperature strength up to 1150°C and resists chemical corrosion at elevated temperatures. In terms of high-temperature engineering, the alloy demonstrates strong resistance to oxidation and carburization. Due to its versatility, Inconel 600 finds applications across various fields with demanding thermo-mechanical and chemical conditions, including the chemical industry, aeronautics, space, and nuclear reactors. The cold-rolled sheet is pickled and annealed at 970°C in a continuous furnace.

**2. 1. 3. Stainless Steel: AISI 321 Steel (14)** AISI 321 steel is also known as austenitic stainless steel due to its titanium content, which prevents corrosion. Type 321

cannot be hardened through thermal treatment, but its strength and hardness can be significantly increased by cold working, despite a reduction in ductility. Annealing: Heat it to 1750 - 2050°F (954 - 1121°C), then water quench or air cool.

The chemical composition, mechanical and thermal properties of the materials used are provided in Tables 1 and 2, respectively. It should be noted that for the copper alloy, chromium (Cr) and zirconium (Zr) contents adhere to the specifications, while other elements are present only in trace amounts.

## 2. 2. Presentation of the Disc Testing

**2. 2. 1. Experimental Procedure** The setup for the disc testing cell is illustrated in Figure 1. The disc testing employs a flat piece with a consistent thickness, closely resembling the thickness of the combustion chamber wall. The disc, embedded at its periphery, is subjected to increasing gas pressure on its bottom face, and the deflection at the midpoint of the upper face is measured. The pressurization rate remains constant throughout the usual rupture tests. The evolution of the gas pressure during the test exhibits three main steps, as illustrated in Figure 2:

- The transient loading period: This results from gradually opening the adjusting valve to achieve the desired gas flow.
- The steady increase in gas pressure: The curve's slope corresponds to the intended loading rate.
- The abrupt drop in gas pressure: This corresponds to the failure of the disc.

The influence of hydrogen on material properties can be measured by comparing results obtained with interstitial helium and deleterious hydrogen. Additionally, this disc testing method offers a wide range of strain rates (from $10^{-6}$ $s^{-1}$ to $10^{0}$ $s^{-1}$) and temperatures (from 300K to 1200K); the prior heating duration is relatively short (about 1.5 hours).

The choice of material components for the disc testing cell depends on the testing temperature and the gas used (inert or harmful). An elastomeric O-ring (see Figure 3) is used for testing the material under inert gas at room temperature; at higher testing temperatures, a metallic O-ring (see Figure 4) must be employed. Because the loading gas should not be contaminated by gases occluded in the O-ring or permeating through the elastomer, the O-ring is also metallic during any environmental testing. The metallic O-ring is not

**TABLE 1.** Chemical composition of the materials studied (spectrum, wt, %)

| Materials studied | C | Cu | Cr | Zr | P | S | Ni | Al | Fe | Si | Ti | Mo | Mn |
|---|---|---|---|---|---|---|---|---|---|---|---|---|---|
| CuCrZr alloy | - | 99 | 0.69 | 0.056 | 0.006 | 0.0013 | 0.006 | <0.002 | 0.007 | <0.005 | - | - | - |
| Inconel 600 | 0.044 | 0.22 | 15.26 | - | - | 0.003 | 75.5 | - | 8.27 | 0.5 | - | - | 0.18 |
| AISI 321 steel | 0.08 | - | 19.00 | - | 0.04 | 0.03 | 12.00 | - | remain | 0.75 | 0.70 | 0.50 | 2.00 |

**TABLE 2.** Mechanical and thermal properties of the materials studied (as it is)

| Materials studied | Young's modulus E [GPa] | Elastic limit σel [MPa] | Fracture limit σf [MPa] | Elongation A [%] | Thermal conductivity λ [Wm-1K-1] | Coefficient of thermal expansion, α |
|---|---|---|---|---|---|---|
| CuCrZr alloy | 120 | 255 | 370 | 18 | 320 | $18.10^{-6}$/K |
| Inconel 600 | 207 | 352 | 693 | 36 | 14.9 | $13.3x10^{-6}$/°C |
| AISI 321 steel | 180 | 276 | 612 | 45 | 16.2 | 17.2 µm/m/°C |

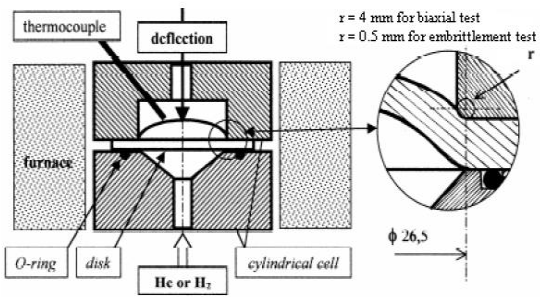


**Figure 1.** Schematic of the used disc testing cell

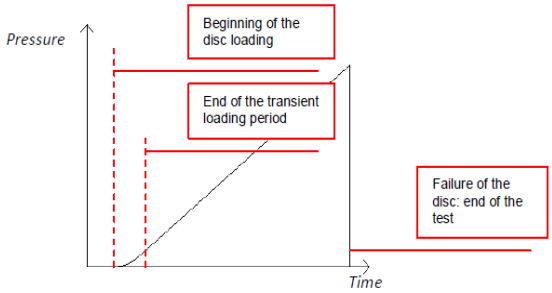


**Figure 2.** Typical evolution of the gas pressure during the disc testing

**Figure 3.** Standardized Elastomeric O-ring

**Figure 4.** Metal O-ring provided by Advanced Products

reusable. The sample and the cell can be heated by an annular resistor furnace. Both the cell and the furnace are insulated with ceramic fiber-based panels and stainless steel sheets (see Figure 7).

**2. 2. 2. Samples** The samples of disc testing are flat discs with constant thickness; the disc thickness is similar to the thickness of the combustion chamber wall to be close to the real material service conditions.

- The disc diameter is 58 mm (see Figure 5).
- The disc thickness is 0.75 mm (see Figure 6).

**2. 2. 2. Disc Testing Equipment** As shown in Figure 7, the disc testing equipment consists of three main subsystems: the tightening system, the gas supply system, and data acquisition. The tightening pressure applied to the periphery of the bottom disc face is provided by a high-pressure hydraulic jack. The pressure amplifier ENERPAC AHB-46, shown in Figure 8, is the core device in the tightening system. This device amplifies the low air pressure (0.4 MPa) up to the high oil pressure (20 MPa), as illustrated in Figure 9. The relative air elasticity is crucial to ensure a nearly constant load on the disc periphery during thermal cycles and subsequent thermal differential deformations.

The gas supply system provides mechanical loading through gaseous pressure and the ambient atmosphere around the disc. Since hydrogen damage can be partially or fully masked if the hydrogen used is not sufficiently pure, adsorbed gases (particularly oxygen and water vapor from the initial ambient atmosphere) must be purged from the supply pipes and downstream volumes. Prior equipment rinsing is achieved through three cycles of alternating filling with pure gas at low pressure (0.1 MPa) and vacuum pumping of the contaminated gas. The loading gas is sourced from a gas cylinder at very high pressure (up to 150 MPa), as shown in Figure 10.

Gas supply is regulated using opening and throttle valves depicted in Figure 11. Gas pressure is measured by a digital pressure sensor with a precision of ±0.1 MPa. The deflection of the disc pole is measured using a Low Voltage Differential Transformer (LVDT) displacement transducer with a precision of ±10 µm. Sample temperature is measured with a thermocouple on the upper disc face. All experimental data are monitored and recorded using a digital plotter (see Figure 12). The sampling period is short enough to capture data at a high rate.

**2. 3. Mathematical modelling of the disc mechanical properties** To calculate the plastic strain and stress at the pole of the disc from the measured deflection and pressure (15, 16), an analytical calculation similar to Hill's method (17) is employed. The calculation of plastic strains and stresses is based on the following assumptions: the stresses are biaxial because the

**Figure 5.** Disc sample with a diameter of 58 mm

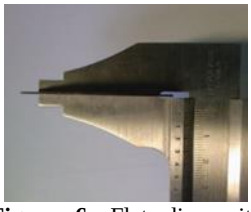

**Figure 6.** Flat disc with constant thickness of 0.75 mm

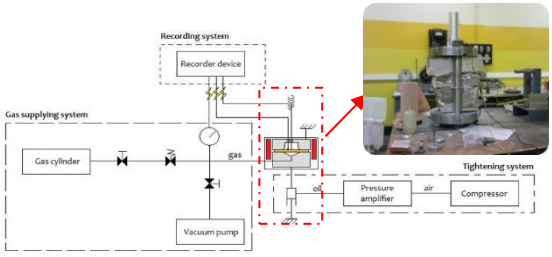


**Figure 7.** Schematic of the disc testing equipment

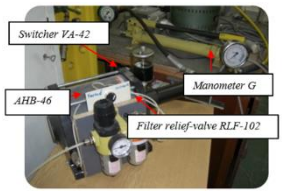


**Figure 8.** Air-oil pressure amplifier ENERPAC AHB-46

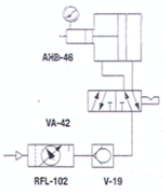


**Figure 9.** Hydraulic diagram of the pressure amplifier

**Figure 10.** Gas storage at high pressure

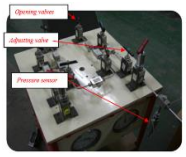

**Figure 11.** Gas supplying

**Figure 12.** Data acquisition Digital plotter SEFRAM 8400

maximum axial stress is the gas pressure, which is negligible in comparison to planar stresses; the material is homogeneous and isotropic, and the volume of a metallic material remains constant during plastic deformation; the thin disc is deformed as a membrane, meaning flexion is neglected at the pole.

The most general mechanical loading involves 6 independent parameters: 3 principal stresses and 3 principal strains. For the disc loading, the axial stress is nullified; the Von Mises stress and strain are calculated from the remaining 5 parameters to facilitate the comparison of results between disc testing and tensile testing. While the Von Mises stress and strain are limiting factors due to the reduction of the disc behavior description from 5 initial parameters to 2, they have consistently enabled coherent comparisons of different mechanical loadings in various applications (18-21). The Von Mises stress and strain are determined from Equations 1 and 2.

Note: The Equations 1 and 2 are referenced in the text, but the actual equations themselves are not provided. Please make sure to include the equations if they are relevant to the context.

$$\bar{\sigma} = \frac{P.\rho}{2.t} \tag{1}$$

$$\bar{\varepsilon} = \ln\left(t_0 / t\right) \tag{2}$$

where : P is the gas pressure, ρ is the cupola radius at the disc pole, t is the pole thickness of the deformed disc and $t_0$ is the initial thickness of the disc.

If the deformed disk is assumed to be a spherical cupola, the pole radius ρ becomes the radius of the sphere. This radius is determined from the deflection W using the geometrical Equation 3 formulated for the outer fiber of the disc (refer to Figure 13). We have confirmed through dimensional measurements that the disc indeed deforms into the assumed spherical cupola.

$$\rho = \left(W^2 + A^2\right) / \left(2.W\right) - r \tag{3}$$

where : W is the deflection at the disc pole, A is the internal radius of the disc embedding and r is the die radius at the disc embedding.

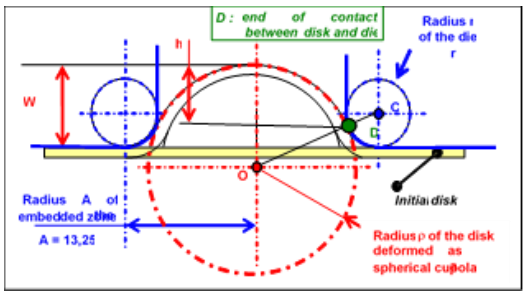


**Figure 13.** Disc deformation-geometrical parameters

The strains at the disc pole are calculated from the deflection W by the analytic Equation 4 based on the above mentioned assumptions; this formula has been validated by measurements of the pole thickness obtained after the deformation of discs made of various materials,

$$\bar{\varepsilon}_i = 2.\int_0^{W_i} \frac{\left[1 - \frac{2.r}{A}.\left(\frac{1}{1+W^2/A^2}\right).\sin\left(2.Arctg\left(\frac{W}{A}\right)\right)\right]}{\rho} dW \tag{4}$$

where : W is the deflection at the disc pole, A is the internal radius of the disc embedding, r is the die radius at the disc embedding and ρ the radius of the disc deformed as a spherical cupola; the radius ρ is calculated from the deflection with the Equation 3.

Testing disc associated to the previous calculation method provides coherent mechanical properties, similar to the usual tensile mechanical properties.

The biaxial tests can be performed at temperatures between 20°C-900°C and at strain rates between $10^{-6}$-$10^{0}$ $s^{-1}$; for instance, the tests can be performed at 900°C at high strain rate (22), which is difficult with another experimental technique.

**2. 4. Flowchart of Rocket Engine Damage** Figure 14 depicts the flowchart of the rocket engine damage procedure, where the combustion chamber undergoes several 'Start-Stop' cycles, rapid cooling, rapid heating, and high temperature gradients, resulting in low cycle fatigue. Similarly, exposure to medium and high temperatures leads to thermal aging and subsequent low cycle fatigue. Furthermore, hydrogen embrittlement and its effects on low cycle fatigue occur. Additionally, the presence of trapped hydrogen contributes to embrittlement and super-saturation, reducing the material's lifespan. When the engine operates at high temperatures in a hydrogen environment, the material absorbs more hydrogen. During engine shutdown, rapid cooling prevents the hydrogen from escaping. Upon restarting, the material experiences plastic deformation at low temperatures and damage due to hydrogen supersaturation. Hydrogen supersaturation significantly reduces the material's lifespan. Another damaging factor

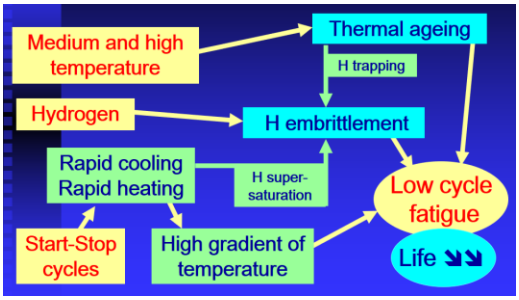


**Figure 14.** Flowchart of rocket engine damage

for the combustion chamber is the thermal aging of alloys resulting from frequent use at medium or high temperatures. These actions are taken to understand and clarify the impacts of hydrogen embrittlement and thermal aging on the fatigue life of a thin-walled circular part, which is a component of a rocket engine.

## 3. RESULTS AND DISCUSSIONS

The results of disc testing are presented in order to reveal the influence of thermal ageing and hydrogen embrittlement on the fatigue life of rocket engines subject to on-off cycles.

**3. 1. Thermal Embrittlement** Thermal ageing is in two types, called stable and unstable thermal of alloys.

**3. 1. 1. Stable Thermal Alloys** For stable stainless steel, ductility increases at the highest temperatures when the rupture deflection increases (see Figure 15). For this alloy, the main phenomenon is the deflection drop at the intermediate temperatures (normalized T = 0.3 - 0.5); this light embrittlement is created by thermal ageing related to atom diffusion and consecutive precipitation; thermal ageing is relatively rapid during mechanical testing due to plastic deformation improves atom mobility; at intermediate temperatures, precipitation appears especially around the grain boundaries.

For the nickel alloy, Figure 15 shows that the fracture elongation changes minimally with temperature, as recrystallization and precipitation occur simultaneously, offsetting their effects. Micrographs confirm that holding at a sufficiently high temperature (T = 0.75 T melting) enhances intergranular precipitation, making it nearly continuous (see Figure 16). The heat treatment of the nickel alloy strengthens intergranular precipitation, rendering it almost continuous.

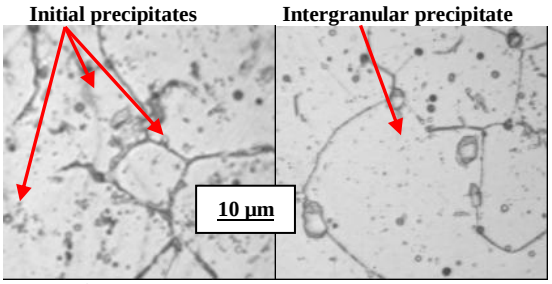


**Figure 16.** Micrographs of the nickel alloy before and after testing at high temperature (results of Figure 15)

**3. 1. 2. Unstable Thermal Alloys** The tested copper alloy (see Figure 17) is initially treated by artificial ageing; this heat treatment at medium temperature gives fine, coherent and well-distributed precipitates, which increases mechanical resistance and decreases ductility. When the material is tested at temperatures higher than the ageing temperature (normalized T ≥ 0.3), the initial precipitates become coarser and less coherent with the matrix; this evolution is more important around the grain boundaries especially at the lowest temperatures; consecutive embrittlement may becomes very significant if the heating duration is long enough. Additionally, the precipitation modification increases the material ductility at normalized temperatures up to 0.35 and decreases the ductility for higher temperatures. The embrittlement increases if the heating duration increases.

For the nickel alloy as shown in Figure 17 is also unstable although it has not been treated by artificial ageing: for this material, the heating duration is great enough to obtain quasi continuous precipitates around the

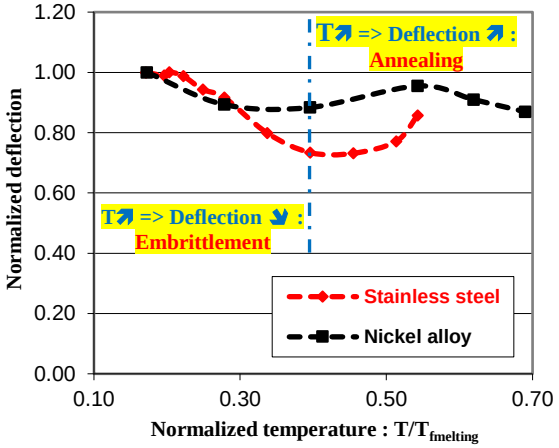


**Figure 15.** Disc testing at different temperatures of stable thermal of alloys

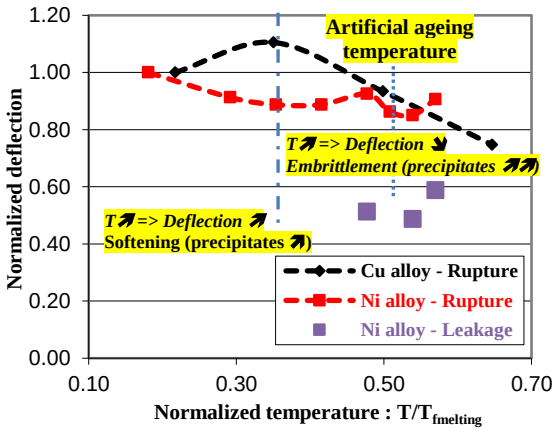


**Figure 17.** Disc testing at different temperatures of unstable thermal of alloys

grain boundaries; under mechanical loading, these precipitates initiate inter-granular cracks and ruptures (see Figure 18). From grain to grain, the cracks propagate along the whole disc thickness and fine gas leakages appear; the leakages are detected by the mass spectrometer, while as they are very fine, the disc can be pressurized until rupture. The leakages are detected at relatively low deflection (see Figure 17); they characterize initiation of metal damage; obviously, tensile testing is not sensitive enough to detect such fine cracking and associate the initiation of damage.

**3. 2. Hydrogen Embrittlement** Hydrogen embrittlement includes two types: Gaseous and internal hydrogen embrittlement.

**3. 2. 1. Gaseous Hydrogen Embrittlement** The two presented cases are influenced on testing temperature and precipitation duration.

**3. 2. 1. 1. Influence of Testing Temperature** The different effects of testing temperature as shown in Figure 19 illustrate:

- At lower temperatures, the copper alloy is hardly sensitive to hydrogen due to fine and coherent precipitates do not trap significant quantities of hydrogen,
- At medium temperatures, the precipitates become coarse and incoherent enough to trap hydrogen with the result that cracks are more easily initiated on the precipitates (23),
- At higher temperatures, the hydrogen embrittlement disappears because it cannot be trapped by the precipitates as it is very mobile.

Concerning the comparison with and without hydrogen, Figure 19 shows that at low temperatures the case without hydrogen is similar to that with hydrogen. However, at medium and higher temperatures the phenomenon observed without hydrogen is less intense than in the presence of this element, as shown by the relative arrow. Finally, in current study observes that this relative arrow decreases at higher temperatures in the case without hydrogen, conversely to the case with hydrogen.

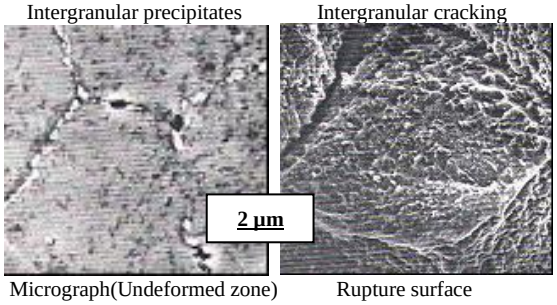


**Figure 18.** Observations of tested discs (results of Figure 5); Nickel alloy tested at T > 0.5$T_{fmelting}$

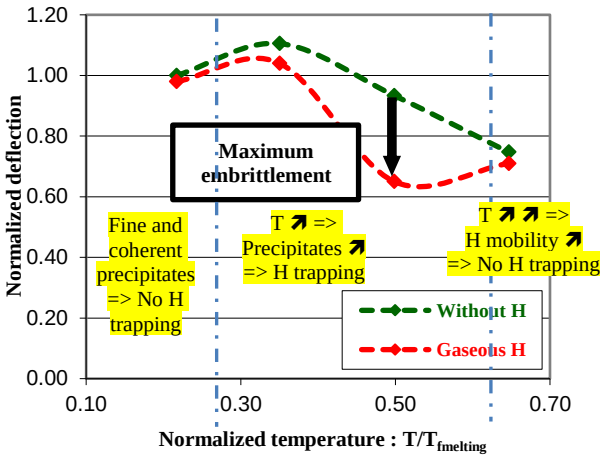


**Figure 19.** Disc testing at different temperatures of stable thermal of copper alloy

Concerning high temperatures, the value of the hydrogen content $C_H$ in the engine wall reaches the hydrogen solubility $S_H$ when steady state of diffusion has been reached. On this subject, Fick's equations give the theoretical time $t_\infty$ to obtain the steady state when a thin wall is subjected to hydrogen on a single face (24):

$$t_\infty = 0.5e^2/D_H \quad (5)$$

where: e is wall thickness (e = 0.75 mm) and $D_H$ is hydrogen diffusivity.

In the case of copper alloy, and to quote an order of magnitude, the steady state is obtained in about 40 s at the temperature of 900 K; however, at this example at high temperature a rocket engine is used during longer periods. During the steady state, hydrogen solubility $S_H$ depends on the absolute temperature T (Arrhenius's law) and on the hydrogen partial pressure $P_H$ (Sieverts's law),

$$S_H = S_0 P_H^{1/2} \exp(-Q/R/T) \quad (6)$$

where: $S_0$ is frequency factor; $P_H$ is hydrogen partial pressure; T is absolute temperature; Q is activation energy and R = 8.31 $Jmole^{-1}K^{-1}$.

However, the hydrogen solubility in copper alloy is identical at 900 K under partial pressure $P_{H900}$ at 600 K under hydrogen pressure $P_{H600} \approx 450\ P_{H900}$ (25).

At 300 K, the hydrogen pressure $P_{H300}$ would have to be much higher than that at 600 K to achieve the same hydrogen solubility. These calculations seem during service at high temperatures, a large amount of hydrogen is introduced into the engine walls; disc testing at room temperature must be performed under high gas pressure to introduce hydrogen into the material with content as high as during service at high temperature.

In addition, when the engine is stopped, it is rapid cooling kept hydrogen trapped on the precipitates that created at high temperatures. When the engine is

restarted, high thermal gradients appear in the thin walls; these gradients create thermal strains in the material while it is super-saturated with hydrogen.

**3. 2. 2. 1. Influence of Precipitation Duration** The thermal embrittlement of the nickel alloy strongly increases for the shortest ageing time (normalized t < 0.2) and its variation is less important for the longest ageing time (see Figure 20). Hydrogen embrittlement is almost identical at any ageing time and the hydrogen effect is added to thermal embritt1ement.

**3. 2. 2. Internal Hydrogen Embrittlement** Figure 21 shows the stable thermal of stainless steel where the hydrogen sensitivity determined at room temperature is almost identical without treatment (normalized T=0.18) or after heat treatment at medium normalized temperature (T = 0.4 - 0.5); the internal hydrogen embrittlement is identical to the gaseous hydrogen embrittlement.

For unstable thermal of stainless steel (see Figure 22), the internal hydrogen embrittlement is more important than for the stable alloy (Figure 21); at medium temperature, the precipitates of the unstable alloy have been modified and they become more efficient to trap hydrogen. For this unstable alloy, the internal hydrogen embrittlement seems more important than the gaseous hydrogen embrittlement; the precipitates trap more hydrogen during charging at medium temperature than during gaseous hydrogen testing at room temperature.

Precipitation evolution during thermal ageing is an important factor of hydrogen embrittlement. Discs tests under gaseous hydrogen may be slightly over-optimistic when they are used to characterize internal hydrogen embrittlement, consecutive to super-saturation during rapid cooling; this super-saturation may be simulated by internal hydrogen charging before mechanical testing.

Comparing Figures 9 and 10, we can say that Internal H embrittlement Unstable stainless steel > Internal H embrittlement Stable stainless steel => H trapping by precipitates (Int H ≈ Gas H in the case of Stable stainless steel et Int H > Gas H in the case of Unstable stainless steel.

The disc testing method, used in conjunction with the previously mentioned calculation approach, yields consistent mechanical properties comparable to those obtained through conventional tensile testing. Both the ultimate strength and proof strength are identical, whether determined through disc testing or tensile testing. The mean values of uniform elongation are also the same for both methods, although there is relatively more significant scattering compared to strength scattering. This elongation scattering is influenced by local deformations initiated by material heterogeneities, such as surface defects (e.g., machining defects) and

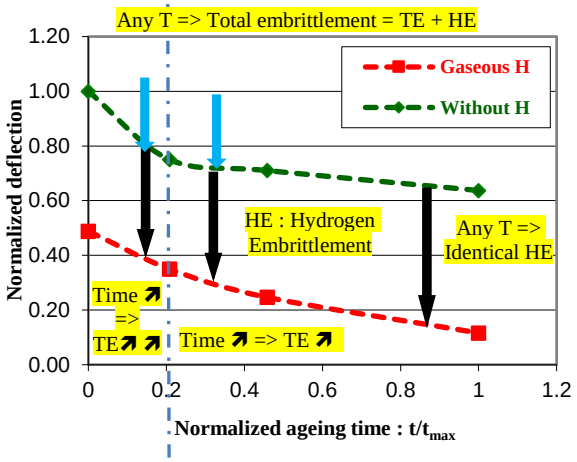


**Figure 20.** Disc testing at 20°C after ageing treatments of Nickel alloy aged at T(K) > 0.5 melting temperature during t < tmax

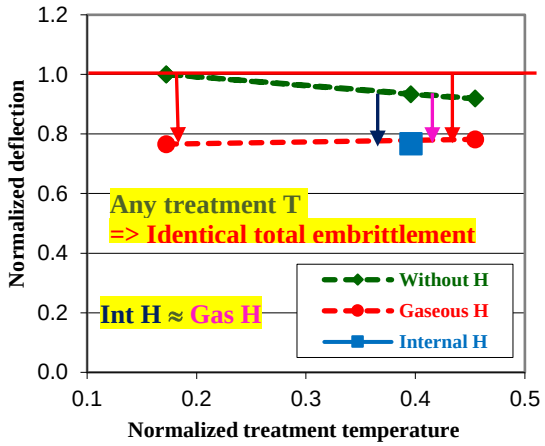


**Figure 21.** Disc testing at 20°C after heat treatment of stable thermal of stainless steel

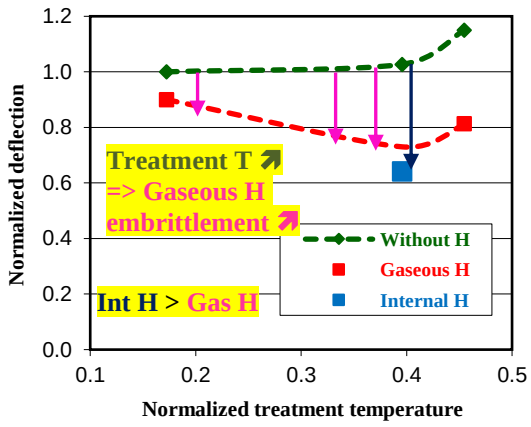


**Figure 22.** Disc testing at 20°C after heat treatment of unstable thermal of stainless steel

metallurgical flaws (e.g., coarse inclusions). These heterogeneities induce area reductions that are detected with differing sensitivities in thick tensile specimens and thin discs. Furthermore, the outer periphery of the disc is not subjected to stress, preventing area reduction from edge defects, as observed in tensile specimens.

The mechanical properties are appropriately correlated with temperature and loading rate-dependent phenomena. At elevated temperatures, the strength of low-alloyed steel diminishes due to dynamic recrystallization during high-temperature deformation. At intermediate temperatures, the material experiences hardening attributed to solute atoms. Notably, hardening is more pronounced in disc testing compared to tensile testing due to distinct strain rates, a crucial hardening factor, in both specimen types.

Biaxial tests can be conducted within a temperature range of 20°C to 900°C and at strain rates from $10^{-6}$ to $10^{0}$ $s^{-1}$. For instance, high-temperature, high-strain-rate tests can be performed at 900°C [26], a task that proves challenging with other experimental techniques. The aforementioned results underscore consistent comparisons between disc testing and tensile testing. As observed in other applications, the Von Mises stress and strain are sufficient for achieving coherent comparisons, even though they reduce the initial set of 6 stresses and strains to only 2 parameters.

**3. 3. Low Cycle Fatigue** Figures 23, 24 and 25 show the influence of themal ageing, influence of gaseous hydrgen and influence of ageing and hydrogen of unstable Ni alloy respectely.

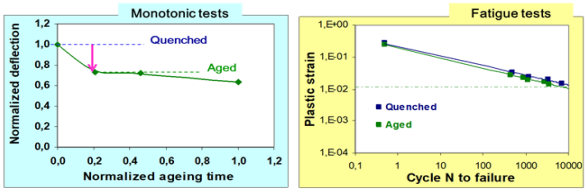


Thermal embrittlement

Strain ≈ 1 % Fatigue life
Quenched : 10000
Aged : 10000

**Figure 23.** Low cycle fatigue : Influence of thermal ageing of unstable Ni alloy

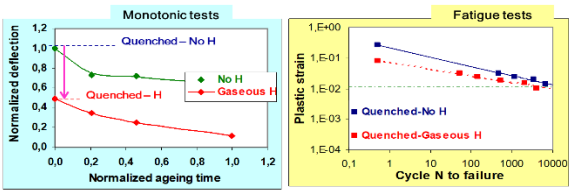


Gaseous H embrittlement

Strain ≈ 1 % Fatigue life
Quenched : 10000
Quenched + H : 8000

**Figure 24.** Low cycle fatigue: Influence of gaseous hydrogen of unstable Ni alloy

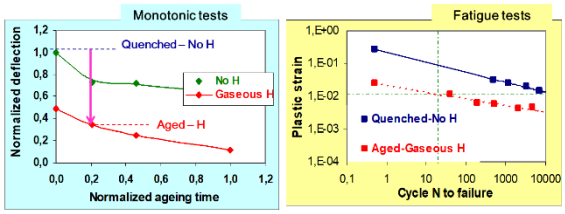


Total embrittlement: Synergy of thermal and hydrogen thermal + gaseous H embrittlement

Strain ≈ 1 % Fatigue life
Quenched : 10000
Aged : 10000
Quenched + H : 8000
Aged + H : 20

**Figure 25.** Low cycle fatigue : Influence of ageing and hydrogen of unstable Ni alloy

Monotonic disc tests showed that the thermally unstable nickel alloy was weakened by thermal ageing and hydrogen. Disc fatigue tests revealed the same phenomena: service life was reduced by thermal ageing and hydrogen gas.

Service life is reduced more by hydrogen than by ageing; this result is logical since hydrogen embrittlement is higher than that obtained by ageing.

Disc fatigue shows the significant synergy between ageing and hydrogen embrittlement ; for a maximum fatigue strain of around $10^{-2}$, the life of a hydrogen-aged material is only 20 cycles, whereas it is around 10000 cycles if the material is damaged only by ageing or only by hydrogen.

When several on-off cycles are applied to the engine, its material subjected to low cycle fatigue; fatigue life may be reduced by the thermal embrittlement and by the hydrogen embrittlement; thus, the life reduction may be mutually amplified by both embrittlements. Fatigue results are not as detrimental for the alloys of rocket engines as for the prior nickel alloy but the phenomena may be similar; consequently, the phenomena must be identified and their influence on the fatigue life must be correctly characterized.

## 4. CONCLUSION

The various results obtained in the present study have led to the following conclusions:

- The fatigue life of rocket engines can be estimated through numerical calculations of damage; before conducting these calculations, both thermal and hydrogen damage must be correctly identified, characterized, and their mutual influence must be verified.
- There is significant synergy between degradation due to thermal aging and embrittlement caused by gaseous hydrogen, as the fatigue life is reduced from 10000 to 20 cycles in alternate fatigue tests at a deformation equal to $10^{-2}$.

- Thermal ageing primarily leads to precipitations around grain boundaries; intergranular precipitates reduce material ductility, particularly if they are nearly continuous.
- While hydrogen damage is minimal under usual service conditions, it might become unacceptable when hydrogen is supersaturated due to rapid cooling, remaining trapped on precipitates formed at elevated temperatures.
- Thermal and hydrogen damage mutually reinforce each other, significantly reducing fatigue life under relatively high deformation.
- In the nickel alloy, leaks occur at higher temperatures ($T(K) > 0.5T_{melting}$) with deflections significantly lower than those obtained at rupture on the same sample.
- For thermally unstable stainless steel, embrittlement induced by hydrogen introduced before mechanical testing is more significant than that obtained under gaseous hydrogen.
- For reduced temperatures from 0.3 to 0.5, intergranular precipitation causes a loss of stainless steel ductility.
- Hydrogen sensitivity is sufficiently low when alloys are hardened by precipitates if they are fine, well distributed and coherent with matrix,
- The precipitate properties depend on chemical composition and thermal exposure consecutive to prior heat treatments or consecutive to services at medium and high temperature,
- The detection of very small leaks through the disc is useful to detect metallurgical evolutions of the material that create relatively short cracks while not changing the macroscopic mechanical properties.

## 5. REFERENCES


1. Zhao N, Zhao Q, He Y, Liu R, Zheng W, Liu W, et al. Investigation on hydrogen embrittlement susceptibility in martensitic steels with 1000 MPa yield strength. Journal of Materials Research and Technology. 2021;15:6883-900. https://doi.org/10.1016/j.jmrt.2021.11.130
2. Moshtaghi M, Loder B, Safyari M, Willidal T, Hojo T, Mori G. Hydrogen trapping and desorption affected by ferrite grain boundary types in shielded metal and flux-cored arc weldments with Ni addition. International Journal of Hydrogen Energy. 2022;47(47):20676-83. https://doi.org/10.1016/j.ijhydene.2022.04.260
3. Chen W, Zhao W, Gao P, Li F, Kuang S, Zou Y, et al. Interaction between dislocations, precipitates and hydrogen atoms in a 2000 MPa grade hot-stamped steel. Journal of Materials Research and Technology. 2022;18:4353-66. https://doi.org/10.1016/j.jmrt.2022.04.094
4. Zheng Z, Liang S, Huang M, Zhao L, Zhu Y, Li Z. Studying the effects of hydrogen on dislocation mobility and multiplication in nickel by phase-field method. Mechanics of Materials. 2022;173:104443. https://doi.org/10.1016/j.mechmat.2022.104443
5. Yu H, Cocks A, Tarleton E. Discrete dislocation plasticity HELPs understand hydrogen effects in bcc materials. Journal of the Mechanics and Physics of Solids. 2019;123:41-60. https://doi.org/10.1016/j.jmps.2018.08.020
6. Wang S, Xu D, Zhang Z, Ma Y, Qiao Y. Effect of electrochemical hydrogen charging on the mechanical behavior of a dual-phase Ti–4Al–2V–1Mo–1Fe (in wt.%) alloy. Materials Science and Engineering: A. 2021;802:140448. https://doi.org/10.1016/j.msea.2020.140448
7. Li P, Wang J, Du M, Qiao L. Hydrogen embrittlement sensitivity of dispersion-strengthened-high-strength steel welded joint under alternating wet-dry marine environment. International Journal of Hydrogen Energy. 2023. https://doi.org/10.1016/j.ijhydene.2023.05.276
8. Wang Q, Liu X, Zhu T, Ye F, Wan M, Zhang P, et al. Mechanism of hydrogen-induced defects and cracking in Ti and Ti–Mo alloy. International Journal of Hydrogen Energy. 2023;48(15):5801-9. https://doi.org/10.1016/j.ijhydene.2022.11.119
9. Momotani Y, Shibata A, Tsuji N. Hydrogen embrittlement behaviors at different deformation temperatures in as-quenched low-carbon martensitic steel. International Journal of Hydrogen Energy. 2022;47(5):3131-40. https://doi.org/10.1016/j.ijhydene.2021.10.169
10. Xu J, Yu C, Lu H, Wang Y, Luo C, Xu G, et al. Effects of alloying elements and heat treatment on hydrogen diffusion in SCRAM steels. Journal of Nuclear Materials. 2019;516:135-43. https://doi.org/10.1016/j.jnucmat.2019.01.019
11. Safyari M, Moshtaghi M, Kuramoto S. Effect of strain rate on environmental hydrogen embrittlement susceptibility of a severely cold-rolled Al–Cu alloy. Vacuum. 2020;172:109057. https://doi.org/10.1016/j.vacuum.2019.109057
12. Metalnikov P, Eliezer D, Ben-Hamu G. Hydrogen trapping in additive manufactured Ti–6Al–4V alloy. Materials Science and Engineering: A. 2021;811:141050. https://doi.org/10.1016/j.msea.2021.141050
13. Liu S, Wu W, Fu H, Li J. Effect of the loading mode and temperature on hydrogen embrittlement behavior of 15Cr for steam turbine last stage blade steel. International Journal of Hydrogen Energy. 2023;48(23):8668-84. https://doi.org/10.1016/j.ijhydene.2022.10.061
14. Lamani E, Jouinot P, editors. Embrittlement phenomena in an austenitic stainless steel: influence of hydrogen and temperature. AIP Conference Proceedings; 2007: American Institute of Physics. 10.1063/1.2733230
15. Genevois-Stasi J. Etude de l'évolution des propriétés mécaniques et métallurgiques de l'inconel 625 au cours du vieillissement, utilisation de l'essai de disques sous pression de gaz. These, Paris. 1998;6.
16. Jouinot P, Gantchenko V, Inglebert G, Riccius J, editors. Material damage induced by environment and temperature and identification process. European Congress on Computational Methods in Applied Sciences and Engineering ECCOMAS 2004; 2004.
17. Hill R. C. A theory of the plastic bulging of a metal diaphragm by lateral pressure. The London, Edinburgh, and Dublin Philosophical Magazine and Journal of Science. 1950;41(322):1133-42. https://doi.org/10.1080/14786445008561154
18. Duncan J. The hydrostatic bulge test as a laboratory experiment. Bulletin of Mechanical Engineering Education. 1965;4:29-37.
19. Aubin V, Quauaegebeur P, Degallaix S, editors. Yield surface behaviour under biaxial fatigue. Proceedings of 8th international fatigue congress, Stockhom, Sweden; 2002.

20. Mesrar R. Comportement plastique des tôles sous sollicitation biaxiale et analyse numérique de la mise en forme par gonflement hydraulique: Metz; 1991.
21. Boulila A, Ayadi M, Zghal A, Jendoubi Ke. Validation expérimentale du modèle de calcul en calotte sphérique des plaques circulaires minces sous l'effet d'un gonflement hydraulique. Mécanique & industries. 2002;3(6):627-38.
22. Jouinot P, Gantchenko V. Lois de comportement mécanique et endommagement de membranes sous pression de gaz. Actes de ITCT, Paris, France. 2006.
23. Örnek C, Mansoor M, Larsson A, Zhang F, Harlow GS, Kroll R, et al. The causation of hydrogen embrittlement of duplex stainless steel: Phase instability of the austenite phase and ductile-to-brittle transition of the ferrite phase–Synergy between experiments and modelling. Corrosion Science. 2023;217:111140. https://doi.org/10.1016/j.corsci.2023.111140
24. McAllester D. On the Mathematics of Diffusion Models. arXiv preprint arXiv:230111108. 2023. https://doi.org/10.48550/arXiv.2301.11108
25. Gale WF, Totemeier TC. Smithells metals reference book: Elsevier; 2003.



Persian Abstract

**چکیده**

در مطالعه حاضر از آزمایش‌های فشار دیسک برای ارزیابی اثرات شکنندگی هیدروژن و پیری حرارتی بر عمر خستگی یک بخش دایره‌ای دیواره نازک در موتور موشک استفاده شد. این تکنیک مقاومت فشار غشاهای آزمایش شده تحت هلیوم و هیدروژن را مقایسه کرد و روشی ساده، حساس و قابل اعتماد ارائه کرد. آزمایش‌های دیسک برای تقلید از شرایط عملیاتی طبیعی انتخاب شدند، زیرا آنها با بخش دایره‌ای با دیواره نازک در موتور موشک هماهنگ هستند. به نظر می رسد اصالت این تست ها در عملکرد بهبود یافته آنها از نظر حساسیت و تکرارپذیری باشد. برای دستیابی به این هدف، آزمایش‌هایی در شرایط مختلف از جمله ضخامت نمونه ۰.۷۵ میلی‌متر، طیف وسیعی از نرخ کرنش از ۱۰–٦ 1-s تا ۱۱۰۰-s، دماهای بین ۲۰ تا ۹۰۰ درجه سانتیگراد و فشار انجام شد. نرخ از ۱۰–۲ تا ۲.۱۰٤ مگاپاسکال در دقیقه. علاوه بر این، مواد مختلفی از جمله مس، آلیاژ نیکل و فولاد ضد زنگ مورد بررسی قرار گرفت. نتایج نشان داد که پیری حرارتی منجر به بارش، به ویژه بارش بین دانه‌ای می‌شود. این رسوبات شکل پذیری مواد را کاهش می دهند، به ویژه زمانی که تقریباً پیوسته باشند. علاوه بر این، حساسیت ماده به هیدروژن زمانی قابل توجه می شود که هیدروژن، فوق اشباع شده به دلیل سرد شدن سریع، روی رسوبات تشکیل شده در دماهای بالا به دام می افتد. علاوه بر این، نتایج نشان داد که آسیب های حرارتی و ناشی از هیدروژن به طور متقابل یکدیگر را تقویت می کنند و در نتیجه باعث کاهش عمر خستگی تحت تغییر شکل زیاد می شود.